Journal of Materials Chemistry A

ROYAL SOCIETY OF CHEMISTRY

PAPER

View Article Online
View Journal | View Issue

Cite this: *J. Mater. Chem. A*, 2025, **13**, 40908

Halide perovskite stabilized in a photoelectrochemical environment by impermeable single crystal TiO_2 for semi-artificial photosynthesis

Choongman Moon,†[a] Chang Hyun Kim,†[a] Jihong Min,†[a] Jaehyuk Koh,[a] Passarut Boonmongkolras,[a] George Kwesi Asare,[bc] Frank Hollmann,[d] Helen Hejin Park,*[bc] Chan Beum Park*[a] and Byungha Shin*[a]

A photoelectrochemical (PEC) device induces electrochemical reactions on the surfaces of light-absorbing semiconductors to harness sunlight for producing valuable chemicals. The most critical issue in PEC devices is the poor stability of semiconductors in electrochemical environments. The stability can be enhanced by applying a transparent and conductive protection layer, which is usually prepared by an oxide thin film with tens of nanometers, on the semiconductor. Nevertheless, ensuring complete impermeability to an electrolyte remains a significant challenge because even a single pinhole in the thin film can lead to the dissolution of the entire underlying semiconductor layer. In this study, we present a facile and reliable protection method applicable to various semiconductors using a thick (200–500 μm) single crystal of TiO_2. The impermeability is ensured by the exceptionally high thickness, without compromising the device performance. We applied the protection layer on a halide perovskite semiconductor well-known for moisture instability, and inductively coupled plasma mass spectrometry rigorously confirmed that there was no dissolution of elements from the halide perovskite film. The robust protection layer also enabled the safe integration of the halide perovskite PEC device and a biocatalyst without concerns about Pb or halide toxicity. An old yellow enzyme from *Thermus scotoductus* (TsOYE) coupled with the PEC device enabled the *trans*-hydrogenation of the C=C bonds, demonstrating the expanded applicability and economic potential of PEC systems for producing fine chemicals and pharmaceutical intermediates.

Received 8th July 2025
Accepted 20th October 2025

DOI: 10.1039/d5ta05513j

rsc.li/materials-a

1 Introduction

Photoelectrochemical (PEC) water-splitting studies aim to integrate essential components of a photovoltaic (PV) system and an electrochemical (EC) system into a unified device with a compact structure. The integration is achieved by immersing an electrode made up of a light-absorbing semiconductor in an electrolyte and forming an electrical junction for separating the photoexcited electron–hole pairs. For a few light-absorbing semiconductors that have band-energy levels favorably aligned with the H_2/O_2 redox potential and exhibit reasonable stability in an electrolyte, they form a solid–liquid junction by making contact with an electrolyte (*e.g.* an n-type Fe_2O_3 photoanode in an alkaline electrolyte) for carrier separation. In most cases, semiconductors either lack favorable band alignment or sufficient stability in an electrolyte; hence, they utilize carrier separating junctions analogous to those of PV systems (*e.g.* p–n junction or carrier-selective contacts). The photo-excited charge carriers separated at the junctions are sent to the surface of the electrodes with EC catalysts to participate in electrochemical reactions. By integrating PV and EC into a single device, PEC systems offer distinctive advantages over a system that electrically connects separate PV and EC systems by eliminating peripheral components.[1,2] However, most PEC devices face stability issues because most semiconductor electrodes are unstable when in contact with electrolytes. A typical approach to enhance stability is by depositing a thin film over the surface of the semiconductor, acting as a protection layer, blocking the permeation of a corrosive electrolyte while allowing the transport of light and electrons.[3] Therefore, an ideal protection layer

[a]*Department of Materials Science and Engineering, Korea Advanced Institute of Science and Technology (KAIST), Daejeon 34141, Republic of Korea. E-mail: byungha@kaist.ac.kr; parkcb@kaist.ac.kr*

[b]*Advanced Materials Division, Korea Research Institute of Chemical Technology (KRICT), Daejeon 34114, Republic of Korea. E-mail: hhpark@krict.re.kr*

[c]*Department of Advanced Materials and Chemical Engineering, University of Science and Technology (UST), Daejeon, 34113, Republic of Korea*

[d]*Department of Biotechnology, Delft University of Technology, Van der Maasweg 9, 2629 HZ Delft, Netherlands*

† C. M., C. H. K., and J. Min contributed equally to this work.

should possess optical transparency, electrical conductivity, electrochemical stability, and impermeability to electrolytes.[4] Arguably, the most successful demonstration of this approach would be TiO_2 thin films protecting Si photoelectrodes. For example, Bae *et al.*[5] demonstrated the stable operation of a silicon photoelectrode in an acidic electrolyte over 40 days without noticeable degradation in its performance. However, preparing a transparent protection layer that is completely impermeable to an electrolyte appears to be challenging. The success of the TiO_2-protected Si photoelectrode is partially attributed to the formation of a stable SiO_2 passivation layer (~1 nm) between the TiO_2 protection layer and the Si light absorber, providing an additional protection effect.[6] Because a single pinhole in the protection layer can cause a catastrophic failure of the device by allowing the permeation of the electrolyte and dissolving the entire semiconductor electrode underneath the protection layer,[7] TiO_2 protection layers on other semiconductors have not been as successful as those on Si photoelectrodes.[7–10]

The challenge posed by an imperfect protection layer becomes more pronounced when using halide perovskites as the PV electrode. Although halide perovskites stand out as one of the most promising light absorbers in the field of PV, their application to PEC devices is severely limited because of their rapid degradation when exposed to moisture. To avoid any exposure to an aqueous electrolyte, most previous halide perovskite PEC studies[11–15] adopted the structure shown in Fig. 1a, in which the semiconductor is protected by a thick and opaque protection layer (*e.g.* stainless steel plates or metal foils with at least hundreds of micrometers thickness) and the light travels through a glass substrate coated with transparent conductive oxide (TCO) on the other side.[16,17] However, in such TCO-front structures, photo-excited charge carriers must travel laterally along the TCO, leading to significant efficiency loss from its resistance. Because the efficiency loss increases with the device area, it becomes detrimental to a PEC device and should be mitigated with surface metallization similar to those of conventional PV cells.[18,19] This metallization typically relies on TCOs or metal grids composed of expensive elements such as silver (Ag) and indium (In). To realize a more compact device structure that avoids the need for surface metallization, structures incorporating a transparent protection layer without the lateral charge transport, as shown in Fig. 1b, need to be investigated. In the electrolyte-front structure, a study was reported in which a halide perovskite was protected against an acidic electrolyte using a transparent TiO_2 thin film protection layer (thickness of 150 nm) prepared *via* the atomic layer deposition (ALD) method.[10] The device was able to carry out a hydrogen evolution reaction (HER) for approximately two hours, which is a remarkably long operation time for a halide perovskite immersed in an electrolyte, but it is still not long enough to make a practical device. Despite the ALD process being known for producing pinhole-free films, even minimal electrolyte permeation must be entirely prevented to enable the construction of durable PEC devices based on halide perovskites. Thus, a transparent and reliable protection layer, regardless of its thickness, should be developed to prepare PEC devices free from the ohmic loss from TCO.

In this study, we employ single-crystal rutile TiO_2 (10 mm × 10 mm × 0.2 mm) to demonstrate an ideal (stable, transparent, conductive, and impermeable) protection layer, through careful optimization of its properties. While TiO_2 is well-known for superior chemical stability, the transmittance and conductivity are enhanced by introducing an anti-reflection coating (ARC) and thermal reduction, respectively. Because no electrolyte can permeate through a rigid crystal with 0.2 mm thickness, the single crystal protection layer should be able to protect various semiconductors when bonded on the semiconductors' surfaces. The single-crystal TiO_2 protection layer was specifically applied to Pb-based halide perovskite, one of the most moisture-sensitive semiconductors, to demonstrate its complete impermeability against electrolyte exposure. To rigorously validate the enhanced stability, we analyzed the concentration of Pb and other ions in the electrolyte, before and after long-term device operation, using inductively coupled plasma-mass spectroscopy (ICP-MS). Our results confirmed that the elements comprising

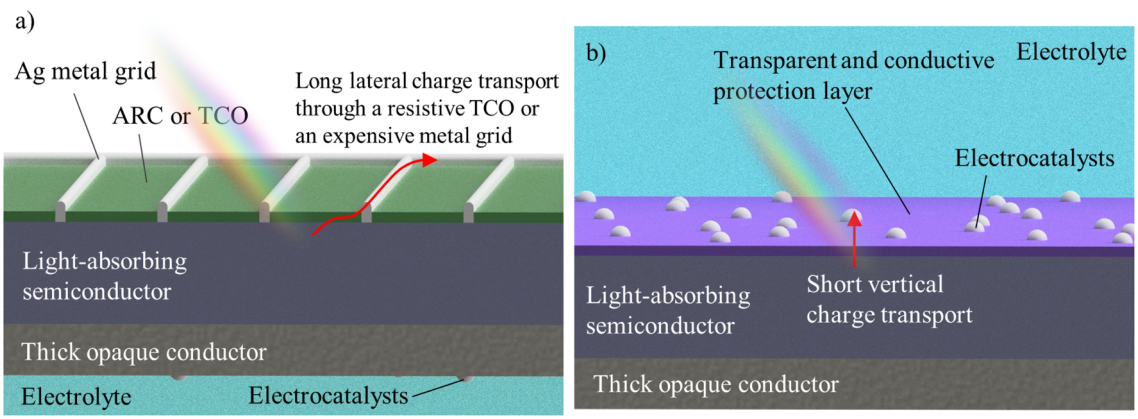

Fig. 1 PEC device structures: (a) TCO-front structure, where the charges are transported in a lateral direction, and (b) electrolyte-front structure with a transparent protection layer, where the charges are transported in a vertical direction. The structure with a transparent protection layer does not require precious elements for TCO or a metal grid, but the transparent protection layer must ensure reliable impermeability against the electrolyte.

the perovskite cell were absent in the electrolyte, thereby affirming the excellent reliability of our protection method. As the TiO_2 protection layer blocks any possibility of toxic Pb contamination in an electrolyte, we were able to use the photoelectrodes for semi-artificial photosynthesis using a biocatalyst. We introduced an old yellow enzyme from *Thermus scotoductus* (TsOYE) to the PEC system for *trans*-hydrogenation of C=C bonds.[20–23] The *trans*-hydrogenation reaction is crucial in the synthesis of fine chemicals and pharmaceuticals, which was highlighted by the 2001 Nobel Prize in Chemistry.[20] Given the significance of this reaction in industrial and pharmaceutical applications, our study demonstrates a promising strategy for leveraging PEC systems beyond conventional water splitting.

2 Result and discussion

The TiO_2 protection layer was prepared by using a rutile crystal (see the Experiment section for details) with dimensions of 10 mm × 10 mm × 0.2 mm (or 0.5 mm). Since pristine TiO_2 is inherently insulating, the electrical conductivity of the protection layer was increased by thermally reducing the crystal[24] and depositing a layer forming an ohmic junction (see Fig. 2a for the procedure for the protection layer preparation). While we found that both aluminum (Al) and indium-doped tin oxide (ITO) provide an ohmic contact to the TiO_2 single crystal (see Fig. S1 for *I–V* measurements from TiO_2 with various contact materials), an ITO film was chosen for device preparation due to its high transmittance. The areal resistivity of the TiO_2 crystal with

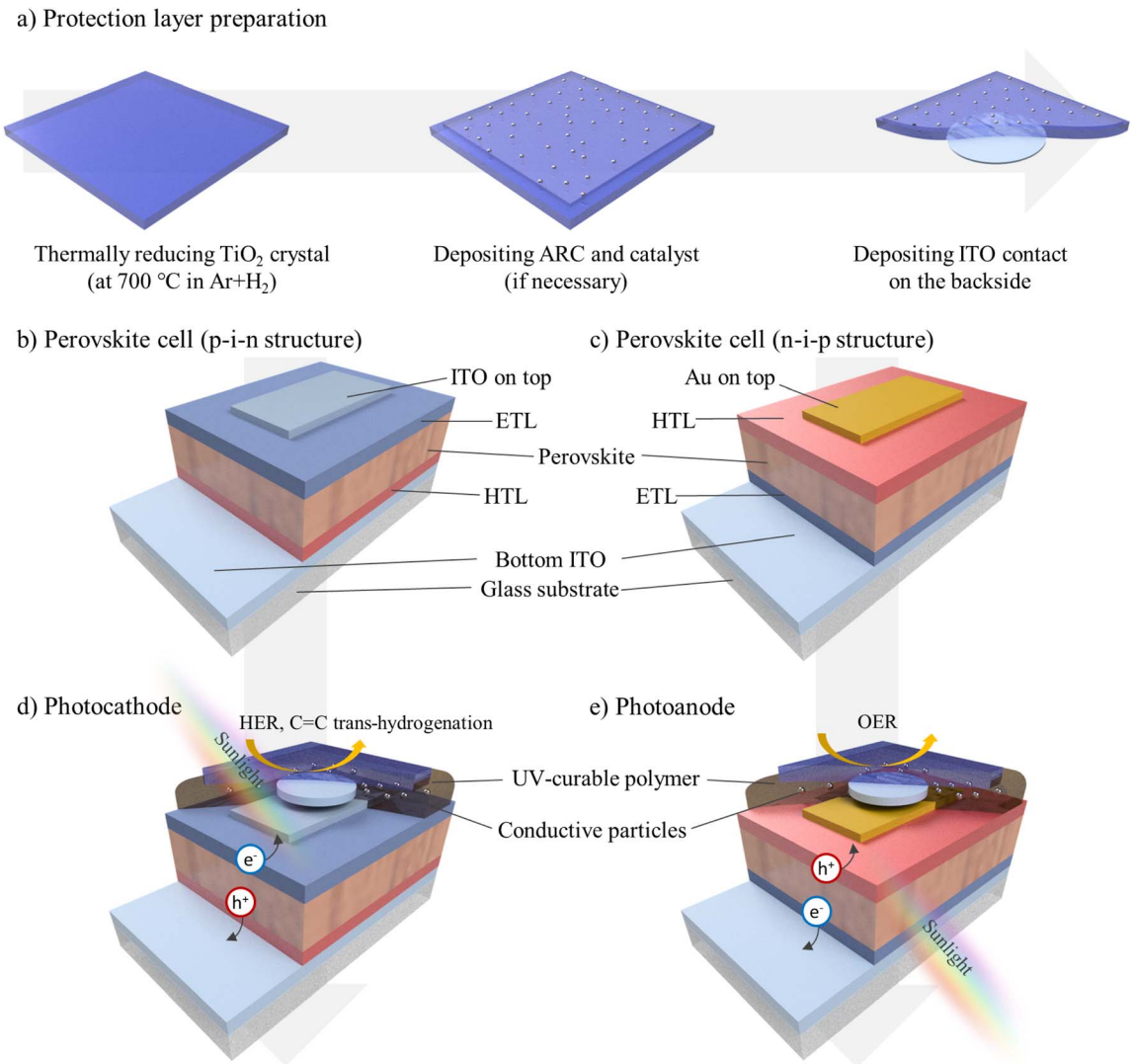

Fig. 2 Schematic of halide perovskite PEC devices. (a) Conductive single-crystal TiO_2 protection layer prepared by thermal reduction, catalyst loading, optional anti-reflection coating (ARC) deposition, and ITO ohmic contact deposition. The TiO_2 with ITO contact was bonded to the perovskite top electrode (ITO or Au) using a transparent conductive adhesive (TCA) comprising a UV-curable acrylate optical adhesive (NOA 86H) containing Ag-coated PMMA beads (~40 μm). The UV-curable adhesive itself is non-conductive; hence, a uniform compressive load during UV cure is applied to establish bead-mediated ohmic contact between the two electrodes. The halide perovskite PV cells in (b) p–i–n configuration (hole transport layer, HTL/perovskite absorber/electron transport layer, ETL) and (c) n–i–p configuration (ETL/absorber/HTL). Halide perovskite (d) photocathode and (e) photoanode prepared from p–i–n and n–i–p structures protected by the TiO_2 protection layer.

200 μm thickness (in units of Ω cm^2) was measured by carrying out *I–V* measurements using Al ohmic contacts on both sides (see Fig. S2a for the *I–V* characteristics). As shown in Fig. S2b, the areal resistivity was reduced to less than 3 Ω cm^2 by increasing the annealing times to more than 12 h. With regards to the optical transmittance, the TiO_2 crystal has reasonably high transmittance over the broad range of the solar spectrum due to its large bandgap (~3.1 eV), but it also needs to minimize the loss from reflection (~30%), and absorption (~10%), as shown in Fig. S3. The loss by absorption is attributed to oxygen vacancies introduced during the thermal reduction (see Fig. S4 for XPS measurements) and can be mitigated by using a thinner crystal, although we have not pursued this due to the limited supply of thinner TiO_2 crystals. The loss by reflection is attributed to the large refractive index mismatch between TiO_2 (~2.7 at the wavelength of 500 nm) and the surrounding medium (water or air) and can be minimized by inducing optical interference destructive to the reflecting wave. We introduced ARC on the side facing the electrolyte and controlled the thickness of the ITO contact on the side facing a semiconductor electrode. We chose a spin-coated SnO_2 thin film as the ARC because its optical refractive index is moderately lower than that of TiO_2 (see Fig. S5a for the refractive indices of SnO_2 and TiO_2), and optimized the thicknesses of SnO_2 and ITO to maximize the transmittance. By optimizing the thicknesses of the SnO_2 (75 nm) and ITO (50 nm) layers, the transmittance of the TiO_2 protection layer at 500 nm was enhanced from 62% to 92%, as shown in Fig. S5b.

Halide perovskite cells were prepared in two different structures with different electrical polarities to make both the photocathode and photoanode. These structures are illustrated in Fig. 2b and c and denoted as p–i–n and n–i–p, respectively, following the convention used in the perovskite photovoltaic community. Both structures include a halide perovskite layer sandwiched between an electron-transporting layer (ETL) and a hole-transporting layer (HTL), covered with an ITO or Au electrical contact on top. The preparation of the PEC device was finalized by covering the contact on top with the TiO_2 protection layer, as shown in Fig. 2d and e. Depending on whether the ETL or HTL faces the protection layer, the as-prepared device can serve as a photocathode or photoanode by transferring electrons or holes to the electrolyte through the protection layer. The bonding between the ITO contact on top of the perovskite cell and the TiO_2 protection layer was made with transparent conductive adhesive (TCA). The TCA was composed of an ultraviolet (UV)-curable polymer (NOA 86H, an acrylate optical adhesive that cures *via* photoinitiated free-radical polymerization under UV light) and conductive particles embedded in the polymer matrix.[25] For the conductive particles, we employed Ag-coated polymethyl methacrylate (PMMA) with a diameter of ~40 μm (Cospheric) because of its well-defined size and shape; however, other conductive materials such as graphite powder should work as well. The liquid-phase UV-curable polymer, sandwiched between the protection layer and the halide perovskite, is cured by UV light to solidify, forming a mechanical bond. During the curing process, uniform pressure was applied over the stack to ensure good electrical contact between the ITO on the TiO_2 and the perovskite cell through the conductive particles. We devised the pressurized curing setup to apply uniform pressure and UV light in a reproducible manner (see Fig. S6 for the structure of the setup). As shown in Fig. S7, the UV-curing process under pressure does not appear to have any short-term or long-term impact on the performance of the halide perovskite cell. We characterized the transmittance and areal conductivity of TCA bonding of two glass substrates or stainless steel plates, depending on the loading of the conductive particles, and we used TCA with particle loading of 2 wt% for device preparation (see Fig. S8 for the conductivity and transmittance of TCA).

To assess the stability of the PEC device protected with a single-crystal TiO_2 protection layer, we carried out unassisted water splitting in an acidic electrolyte (0.5 M H_2SO_4) by using the as-prepared halide perovskite photocathode and photoanode for HER and OER, respectively. Platinum (Pt) or iridium (Ir) was deposited on the protection layer for the photocathode or photoanode to enhance the HER or OER activity. The HER and OER activities of the electrocatalysts on the TiO_2 protection layers were also characterized, and their Faraday efficiencies, determined using gas chromatography (GC), were also close to 100% (see Fig. S9 for the GC measurements). The perovskite PEC devices were electrically connected in series and characterized by using a PEC reactor for optically parallel tandem measurements,[26] as shown in Fig. 3a. The cyclic voltammetry curves from each photoelectrode under AM 1.5 G simulated sunlight are shown in Fig. 3b. Because the halide perovskite layer was not damaged, compared to the electrocatalysts in the dark, the cyclic voltammetry from the photoelectrodes shifts by an amount equivalent to the photovoltage produced by the halide perovskite cells: 1.1 V from each photoelectrode.

For comparison, we also characterized the halide perovskite photocathode without the TiO_2 single-crystal protection layer (with only Pt catalysts deposited on the ITO layer of the p–i–n perovskite cell) or with a TiO_2 thin film protection layer prepared by e-beam evaporation (100 nm TiO_2 thin film and Pt catalysts deposited on the ITO layer of the perovskite cell with the p–i–n structure). In these cases, their performances degraded rapidly over several cycles of cyclic voltammetry (CV) measurements carried out in less than 10 minutes because the moisture-sensitive halide perovskite layers were poorly protected against the electrolyte (see Fig. S10 for the CV from devices without the single-crystal TiO_2 protection layer). Because the single-crystal TiO_2 protection layer introduced in this study is exceptionally thick and does not have any pinholes, it did not allow any leakage of the electrolyte and enabled the stable operation of the photocathode and photoanode. As anticipated from the crossover of the illuminated CV traces in Fig. 3b and the two-electrode CV of the tandem PEC device shown in Fig. S11, the device drives unassisted overall water splitting under 1-sun illumination at zero applied bias, achieving an STH of 5.06% (see the inset of Fig. 3c). Note that the sum of the active areas of both the photocathode and photoanode was used for normalizing the current density in the plot due to the optically parallel design of the PEC reactor.

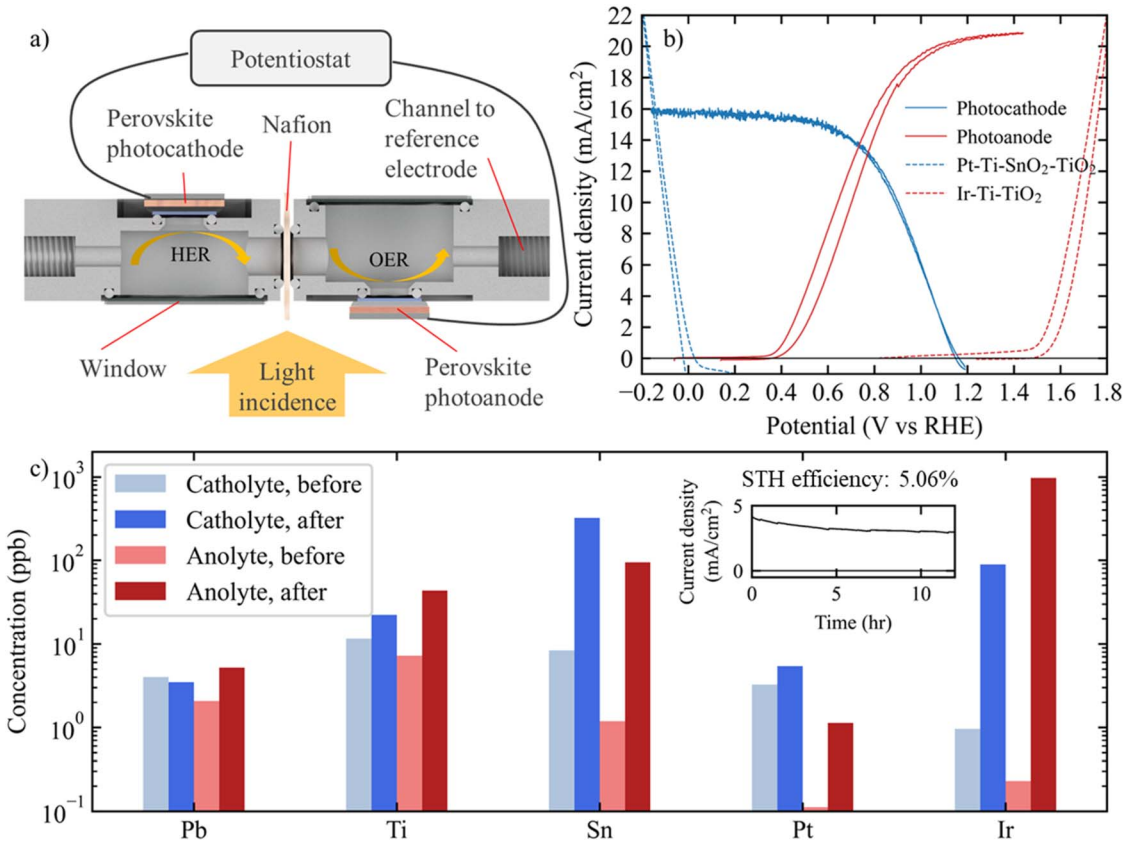

Fig. 3 Photoelectrochemical water-splitting using halide perovskite PEC devices (operation in 0.5 M H_2SO_4 acidic electrolyte, AM 1.5 G, 100 mW cm^{-2}) (a) schematic of the PEC reactor used for characterizing the parallel tandem PEC device. (b) Cyclic voltammetry plots of halide perovskite photocathode (solid blue) and photoanode (solid red) under 1 sun illumination in comparison with the TiO_2 protection layers decorated with electrocatalysts for the HER (dotted blue) or OER (dotted red) in the dark. Note that the sign conventions for cathodic reactions (photocathode and the HER catalyst) are reversed. (c) Concentration of elements before and after 12 hours of unbiased water-splitting by the halide perovskite tandem PEC device (inset: chronoamperometry data from the unbiased water splitting).

We prepared the photoelectrode on an ITO-coated glass substrate despite its resistance because ETL, HTL, and halide perovskite deposition processes require delicate optimization, considering the adhesion and chemical compatibility between the layers. In order to study a halide perovskite PEC device without the lateral charge conduction through TCO, we prepared a photocathode on a titanium substrate. The photocathode on the titanium substrate exhibited CV comparable to that prepared on ITO glass, as shown in Fig. S12. In the case of the photoanode, the opaque Au contact is deposited on the p-type side facing the electrolyte because a contact with a large work function is needed. Thus, the photoanode is positioned so that the ITO side faces the light source (as shown in Fig. 1a), although the ohmic loss from ITO is inevitable in this structure. In order to show that the single-crystal TiO_2 protection layer is applicable to a photoanode with the electrolyte side facing the light source (as shown in Fig. 1b), we prepared a silicon photoanode protected by the TiO_2 protection layer, as shown in Fig. S13.

To demonstrate the complete impermeability of the TiO_2 protection layer, we measured the concentration of selected ions in the electrolyte, before and after 12 hours of unassisted water-splitting, using inductively coupled plasma-mass spectroscopy (ICP-MS), as shown in Fig. 3c (see Table S2 for details on the ICP-MS measurement). The stability assessment using ICP-MS provides a direct and highly sensitive determination of the device stability by detecting elements dissolved from components comprising the electrode at the parts-per-billion (ppb) level. The concentration of Pb ions in the electrolyte remained unchanged, which indicates that the Pb-based halide perovskite layer was not damaged by the electrolyte at all. On the other hand, the concentrations of Sn, Pt, and Ir increased after the stability test as the electrocatalysts and ARC were exposed to the electrolyte. It is worth noting that the stability of the electrocatalysts is comparable to that in the previous study.[27] The stability number (the ratio between the number of gas molecules produced and metal ions dissolved) of metallic Ir was found to be 1.6×10^4 from the ICP-MS measurements, which is in the range of the stability numbers of 10^3–10^5 of metallic Ir reported in the previous study.[27] Thus, the stability of the PEC system investigated in this study is comparable to those of electrocatalysts, not the halide perovskite, as the single-crystal TiO_2 provides complete protection.

As the elements possessing biological toxicity, such as Pb and halides, are fully encapsulated by the single-crystal TiO_2 protection layer, this study offers the potential to couple the

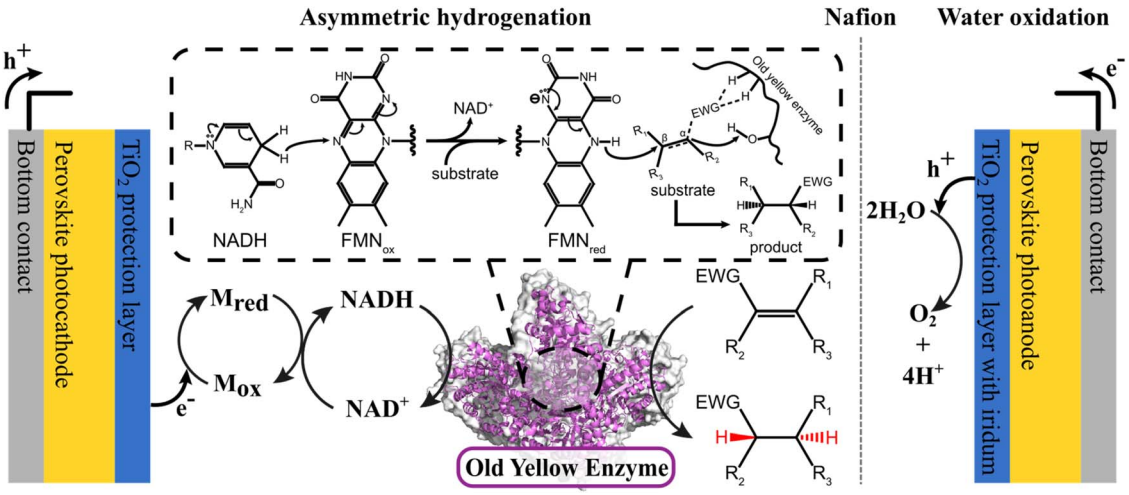

Fig. 4 Illustration of the unbiased PEC biocatalysis using TiO_2-protected halide perovskite photocathode. The photocathode generates photoexcited electrons for the regeneration of M_{red} and NADH cofactors. The enzymatically active NADH donates a hydride to a prosthetic group (*i.e.*, flavin mononucleotide, FMN) in TsOYE. The reduced FMN donates a hydride onto Cβ of an enzymatic substrate while a Tyr-residue supplies a proton to Cα, resulting in the *trans*-hydrogenation of the C=C bond.

halide perovskite electrode with biocatalysts for semi-artificial photosynthesis. Biocatalyst-integrated PEC (BPEC) systems enable highly selective transformations for the production of valuable fine chemicals and pharmaceuticals, greatly enhancing economic feasibility and sustainability.[28–34] Thus, we introduced a TsOYE to the PEC system for the *trans*-hydrogenation of C=C bonds,[22,23] which is crucial in the synthesis of fine chemicals and pharmaceuticals. In the BPEC system (see

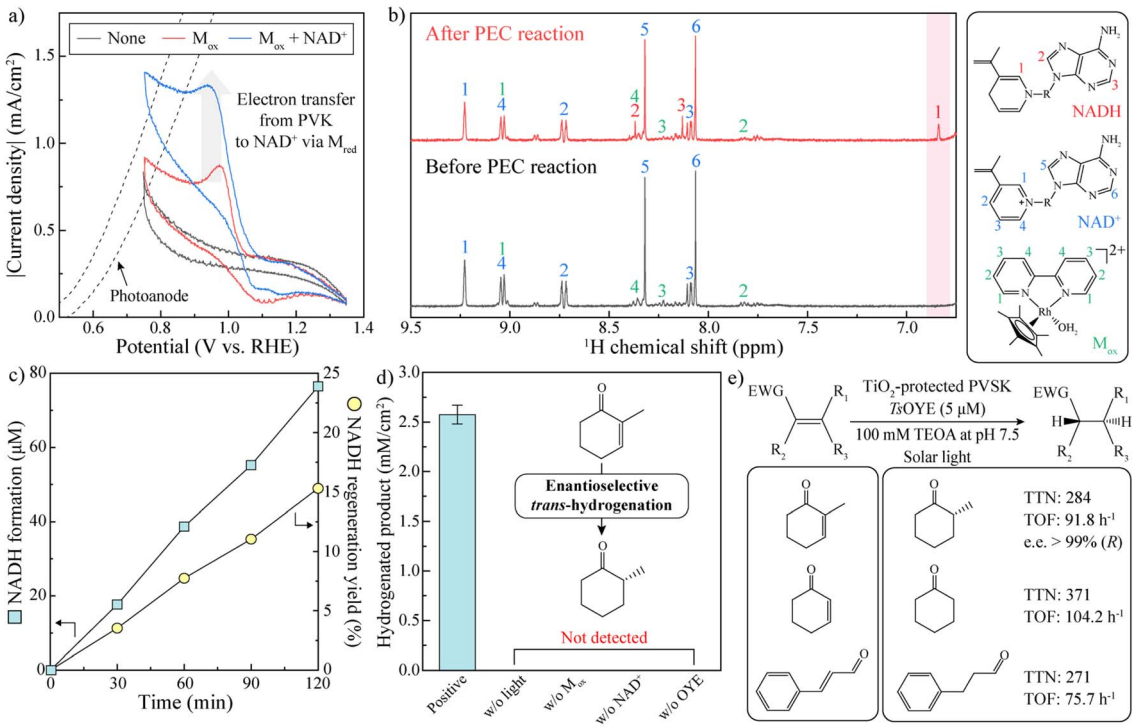

Fig. 5 Biocatalytic photosynthesis using a TiO_2-protected halide perovskite tandem device. (a) Cyclic voltammograms of the photocathode for NAD^+ reduction. (b) ^1H nuclear magnetic resonance spectra before and after the photoelectrocatalytic reaction. The molecular structures of NADH, NAD^+, and M_{ox} are shown in the right panel. Reaction time: 2 h. (c) PEC regeneration of NADH from NAD^+ using the TiO_2-protected halide perovskite tandem device. (d) Control experiments of enantioselective photobiocatalytic hydrogenation using TsOYE. (e) Enzymatic substrate scope of the TsOYE-driven hydrogenation. The solvent of the cathodic electrolyte: triethanolamine (TEOA)-buffered solution (100 mM, pH 7.5). Anodic electrolyte: potassium phosphate buffer (100 mM, pH 7.5). Light conditions: 1 sun illumination (AM 1.5 G, 100 mW cm^{-2}). Reaction time: 8 hours.

Fig. 4 for the overall reaction scheme), the structure and electrochemical reaction of the photoanode remain the same as in the unassisted water-splitting experiment, and the photocathode reduces an Rh-based electron mediator $[Cp^*Rh(bpy)H_2O]^{2+}$ (M_{ox}; $Cp^* = C_5Me_5$, bpy = 2,2′-bipyridine) to regenerate M_{red} in a neutral electrolyte. M_{red} can selectively reduce NAD^+ to enzymatically active 1,4-NADH, without the formation of the enzymatically inactive 1,6-NADH or NAD_2 dimer,[21,35] and the 1,4-NADH-dependent TsOYE ene-reductase invokes the *trans*-hydrogenation reaction in turn.

A series of electrochemical and spectroscopic measurements was carried out to validate the chemical production through BPEC. Cyclic voltammograms show a photocathodic current of M_{ox} near the applied bias of 0.9 V *vs.* RHE, which is attributed to the reduction of M_{ox} on the surface of the TiO_2-protected halide perovskite (see Fig. 5a for CV with or without M_{ox}, NAD^+). The photocathodic current further increased with the addition of NAD^+, indicating the successive transfer of electrons from the photoelectrode to NAD^+ *via* M_{ox}. As expected from the intersection of *I–V* plots from the photocathode and photoanode overlaying each other (see Fig. 5a and S14a for the *I–V* plots), the unbiased coupling of the photoelectrodes enabled NADH regeneration and OER. The ^1H nuclear magnetic resonance spectrum showed a characteristic peak at 6.94 ppm for NADH after the unbiased photoelectrolysis, confirming the conversion of NAD^+ to NADH using M_{ox} (see Fig. 5b and S15). The regeneration rate of NADH was 38.7 μM cm^{-2} h^{-1} (that is, 15.3% of NADH was regenerated) but became negligible in the absence of M_{ox}, NAD^+, or light (see Fig. 5c and S16). By introducing NADH-dependent ene-reductase from TsOYE, we carried out asymmetric hydrogenation reactions. The exposure of the tandem device to solar light drove the reduction of 2-methyl-2-cyclohexen-1-one to enantiopure (*R*)-2-methylcyclohexanone [>99% enantiomeric excess (e.e.)] with a rate of 0.184 mM h^{-1} and a turnover frequency (TOF) of 91.8 h^{-1} (see Fig. 5d and S17). The BPEC system halted at around 8 h because prolonged exposure of TsOYE to irradiated sunlight may decrease its activity (see details in the caption of Fig. S18). The control experiments lacking light, M_{ox}, NAD^+, or TsOYE did not produce any hydrogenated products, verifying that the reaction was driven by the successive charge transport *via* M_{ox}, NAD^+, and TsOYE. To demonstrate broader applicability, we expanded the enzymatic substrate scope of the TsOYE-catalyzed hydrogenation reactions (Table S3) to include the production of cyclohexanone [TOF = 104.2 h^{-1}, turnover number (TTN) = 371] and 3-phenylpropionaldehyde (TOF = 75.7 h^{-1}, TTN = 271) as shown in Fig. 5e and S19.

3 Conclusion

A practical PEC device requires a reliable protection layer, which should be chemically stable, electrically conductive, optically transparent, and impermeable to the electrolyte. In this study, we present a novel approach to prepare a protection layer that satisfies these conditions by using a single-crystal TiO_2. While the TiO_2 crystal is intrinsically stable in an electrochemical environment, we thermally annealed the crystal in a hydrogen atmosphere to increase the conductivity (<3 Ω cm^2) and introduced the SnO_2 ARC to enhance the optical transmittance (>90% at 550 nm). To demonstrate the complete impermeability of the protection layer, we applied it to a Pb-based halide perovskite, which exhibits serious instability when exposed to moisture, despite its exceptional optoelectronic properties. Both photocathode and photoanode were prepared by combining the protection layer and halide perovskite films using TCA, and we carried out unassisted PEC water-splitting using these photoelectrodes. Since the halide perovskite layers were successfully protected by the TiO_2 protection layer, they remained intact in the electrochemical environment, as demonstrated by the ICP-MS measurement on the concentration of Pb in the electrolyte before and after the water-splitting reaction. By successfully protecting the Pb-based halide perovskite, we improved the economic viability of PEC by carrying out semi-artificial photosynthesis using TsOYE for *trans*-hydrogenation without concern for the toxicity of Pb. Our BPEC device demonstrated high efficiency and enantioselectivity in the biotransformation of various enzymatic substrates into value-added products (TTN = 1290 cm^{-2}, TOF = 418 h^{-1} cm^{-2}, and e.e. > 99%).

4 Experiment

4.1 Single-crystal TiO_2 protection layer preparation

Single-crystal TiO_2 (rutile, [100], 10 mm × 10 mm × 0.2 or 0.5 mm) was purchased from MTI Corporation. To the best of our knowledge, anatase crystals with similar dimensions are limited in supply. The crystal was cleaned in a Piranha solution (a mixture of H_2SO_4 98% and H_2O_2 30% in a 3 : 1 ratio) overnight, followed by rinsing with Milli-Q water (18.2 MΩ cm). After cleaning, the crystal was annealed in a tube furnace filled with 300 mTorr of Ar + H_2 (3.9%) at 700 °C for 6 hours, unless otherwise noted. On the side of the TiO_2 crystal that will be in contact with the electrolyte, ARC or an electrocatalyst was coated if needed. ARC is a thin layer of SnO_2 prepared by spin-coating $SnCl_2 \cdot 2H_2O$ dissolved in ethanol at 2000 rpm for 30 s, followed by subsequent annealing using a hot plate at 300 °C for 20 min. The thickness of the SnO_2 ARC was controlled by the concentration of the chemical precursor, and ellipsometry measurements show that a concentration of 300 mM provided a thickness of ∼75 nm (see the inset in Fig. S5a for the SEM image of the SnO_2 thin film coated on the TiO_2 crystal). For the HER or OER reaction, the Ti adhesion layer and Pt (for HER) or Ir (for OER) were deposited using an electron beam evaporator. The nominal thicknesses of Ti, Pt, and Ir were 1, 1, and 20 nm, respectively. When carrying out a biocatalytic reaction, a bare TiO_2 surface was exposed to the electrolyte without any catalyst or ARC. On the backside in contact with a perovskite cell, ITO was deposited by radiofrequency magnetron sputtering, and the thickness was maintained at ∼50 nm to maximize the transmittance of the protection layer.

4.2 Halide perovskite PV cell preparation

The halide perovskite PV cells with either p–i–n or n–i–p structure were prepared for the photocathode or photoanode.

Due to their different stack order, the materials and fabrication processes for each structure were individually optimized with careful consideration of interfacial adhesion and chemical compatibility.

The halide perovskite PV cell with the p–i–n structure (bandgap: 1.7 eV) for the photocathode was prepared on an ITO substrate. 17 nm-thick NiO_x was first deposited on the ITO substrate using radiofrequency sputtering. Poly(triaryl amine) (PTAA, 5 mg mL^{-1} in toluene) was spin-coated on the NiO_x film at 6000 rpm and then annealed at 100 °C on a hot plate for 10 min. Perovskite (1.4 M in DMF and NMP mixed solution) solution with a composition of $FA_{0.65}MA_{0.2}Cs_{0.15}Pb(I_{0.8}Br_{0.2})_3$ was spin-coated on the PTAA film at 3000 rpm for 10 s, then immediately immersed in a diethyl ether (DE) bath for 30 s. In the DE bath, the yellowish film was converted to a dark brown color, indicative of the formation of crystalline perovskite. After bathing, the film was annealed at 100 °C for 3 min. A 30 nm-thick C_{60} layer was deposited on the perovskite film using a thermal evaporator, and then polyethyleneimine (PEIE, 0.2 wt% in methanol) was spin-coated at 4500 rpm. Finally, 70 nm-thick ITO was deposited on the C_{60}/PEIE film using radio-frequency sputtering. All the spin-coating processes for the halide perovskite cell were done in a glove box (N_2 atmosphere).

The halide perovskite PV cell with the n–i–p structure (bandgap: 1.55 eV) for the photoanode was also prepared on an ITO substrate. The ITO glass substrates were systematically washed in deionized water, acetone, and isopropyl alcohol, respectively, for 15 minutes during each washing process. After washing, the ITO glass substrates were dried in a 100 °C oven for 5 minutes. NP-SnO_2 was prepared by mixing Sukgyung gel SnO_2 solution and deionized water in a ratio of 1 : 5, respectively. The resulting solution was spin-coated onto the glass/ITO substrate at 3000 rpm for 30 seconds, followed by annealing of the substrate at 150 °C for 1 hour. The perovskite precursor solution was synthesized by dissolving 800 mg of $FAPbI_3$, 30 mg of MACl, and 30 mg of $MAPbBr_3$ in a mixed solvent of DMF/DMSO (in a ratio of 8 : 1 v/v). The resulting $(FAPbI_3)_{0.95}(MAPbBr_3)_{0.05}$ perovskite precursor solution was spin-coated onto the glass/ITO/np-SnO_2 substrate at 500 rpm for 5 seconds, 1000 rpm for 8 seconds, and 5000 rpm for 12 seconds. During the final state, ethyl acetate anti-solvent was dripped onto the perovskite precursor at 12 s, followed by annealing at 100 °C for 1 hour and then 150 °C for 4 minutes, respectively. PTAA solution with OATFSI as an additive was prepared by dissolving in toluene and then spin-coated on top of the perovskite films at 3000 rpm for 30 seconds. Finally, an Au top electrode was deposited with a thermal evaporator with a power of 0.98 W on top of the PTAA layer to complete the perovskite solar cell devices.

4.3 Bonding the single-crystal TiO_2 protection layer and the halide perovskite cell

The single-crystal TiO_2 protection layer was attached to the perovskite cells by using a transparent conductive adhesive (TCA). The TCA was prepared by mixing Ag-coated PMMA particles (purchased from Cospheric LLC) and a UV-curable polymer (NOA 86H). The TCA sandwiched between the TiO_2 and halide perovskite cell was cured with an LED light (wavelength: 420 nm) through the TiO_2 under uniform mechanical pressure. To ensure the uniformity of the pressure, we devised a pressurized curing setup (see Fig. S6 for details on the setup).

4.4 Water-splitting photocathode and photoanode

The parallel tandem PEC device made up of the halide perovskite photocathode and photoanode was characterized by using a homemade PEC reactor. The photoelectrodes were fixed on the wall of the PEC reactor with only the TiO_2 protection layers exposed (with ARC and electrocatalysts if used) to the electrolyte in the PEC reactor through O-rings between the devices and the reactor. The active area of the photoelectrodes determined by the optical apertures was 0.22 cm^2 each. For 3-electrode characterization, a separate chamber with a reference electrode (Ag/AgCl in 3 M KCl) was connected to a PEC reactor, and a Pt wire was placed into the chamber as a counter electrode. Unassisted water-splitting reactions were carried out by short-circuiting the photocathode and photoanodes under simulated sunlight (a xenon lamp with an air mass 1.5 G filter). Before and after the unassisted water-splitting for 12 hours, the concentrations of the elements in the electrolyte were determined by ICP-MS.

4.5 Synthesis of Rh-based redox mediator (M_{ox})

The redox mediator, $[Cp^*Rh(bpy)H_2O]^{2+}$ (M_{ox}; $Cp^* = C_5Me_5$, bpy = 2,2′-bipyridine), was prepared by mixing a solution of the Rh-containing precursor with the bipyridine ligand. We dissolved 47 mM pentamethylcyclopentadienylrhodium (PCD) chloride dimer (97%; Sigma-Aldrich) and 160 mM 2,2′-bipyridine (>99%; Sigma-Aldrich) in 8 mL and 5 mL of methanol, respectively. After 30 min of sonication, we added the bipyridine solution dropwise to the PCD solution with gentle stirring. After stirring for 1 hour, we mixed the solution with 65 mL of diethyl ether and stored it at 4 °C for 24 hours. Precipitated powder was collected by vacuum filtering and washed with diethyl ether three times. Finally, we dried the precipitate under a vacuum at room temperature for 16 hours.

4.6 Photoelectrocatalytic regeneration of NADH

We investigated the capacity of the TiO_2-protected halide perovskite photocathode for the regeneration of NADH in a 3-electrode configuration, which is consistent with the characterization for water-splitting. β-Nicotinamide adenine dinucleotide hydrate (NAD^+, >96.5%) was purchased from Sigma-Aldrich Corp. (USA) and used without further purification. We prepared an electrolyte solution by adding M_{ox} and NAD^+ in a potassium phosphate (KPi) buffer (100 mM, pH 7.5). We quantified NADH using a V-650 UV-vis absorption spectrophotometer (JASCO Inc); the absorption peak position and the molar extinction coefficient of NADH were 340 nm and 6220 M^{-1} cm^{-1}, respectively. We recorded ^1H nuclear magnetic resonance (^1H NMR) spectra using a 400 MHz AVANCE NEO (Bruker) spectrometer to corroborate the regeneration of NADH.

4.7 Preparation of the OYE from *Thermus scotoductus* (TsOYE)

We obtained TsOYE from *E. coli* BL21 (DE3) cells harboring the pET22b(+) plasmid.[22,36] 1 L of autoinduction media supplied with 100 μg mL^{-1} of ampicillin was incubated overnight at 30 °C. The cell pellet was collected by centrifugation for 20 min at 4 °C and 10 000×*g* and washing with 20 mM MOPS buffer with 5 mM $CaCl_2$. The cell was suspended in a buffer and lysed with a Multi Shot Cell Disruption System (Constant Systems Ltd, UK). After removing cell debris by centrifugation, we purified the enzyme by incubating the supernatant at 70 °C for 1.5 hours. We separated the precipitated proteins by centrifugation for 30 min at 4 °C and 8000×*g*. A bright-yellow solution of TsOYE (>90% pure as estimated by sodium dodecyl sulfate polyacrylamide gel electrophoresis analysis) was concentrated using an Amicon® Ultra-15 Centrifugal Filter Device (cut-off 30 kDa), followed by desalting using a PD-10 Desalting Column (GE Healthcare). The final solution was freeze-dried for long-term preservation.

4.8 Unbiased biocatalytic hydrogenation with the halide perovskite PV cell

PEC biocatalysis was coupled with the regeneration of NADH using the parallel tandem device with the 2-electrode configuration. We prepared a cathodic electrolyte solution by dissolving 5 μM TsOYE, enzyme substrate, $CaCl_2$, M_{ox} (0.25 mM), and NAD^+ (1 mM) in an O_2-depleted triethanolamine (TEOA) buffer (100 mM, pH 7.5). We used KPi buffer (100 mM, pH 7.5) as an anolyte solution. The geometrical surface areas of the TiO_2-protected halide perovskite photoelectrodes were 0.2206 cm^2. After 8 hours of PEC biocatalytic reaction, we collected 50 μL of the sample and mixed it with ethyl acetate (containing 5 mM 1-octanol as the internal standard) to extract the hydrogenated products. We obtained calibration curves from the area ratio of the target analytes to the internal standard (see Fig. S20 for calibration curves), and then quantified the enzymatic products using a 7890 A gas chromatograph (Agilent Technologies Inc.) equipped with a CP-Chirasil-Dex CB column (25 m, 0.32 mm, 0.25 μm). The enantiomeric excess (e.e.), total turnover number (TTN), and turnover frequency (TOF) of TsOYE were calculated according to eqn (1)–(3), respectively.

$$\text{e.e.} = \frac{|\text{Moles of an enantiomer} - \text{Moles of the other enantiomer}|}{\text{Total moles of product}} \times 100 \quad (1)$$

$$\text{TTN}_{\text{TsOYE}}(\text{cm}^{-2}) = \frac{\text{Maximum concentration of product}}{\text{Concentration of TsOYE} \times \text{surface area}} \quad (2)$$

$$\text{TOF}_{\text{TsOYE}}(\text{h}^{-1}\ \text{cm}^{-2}) = \frac{\text{Turnover number of TsOYE}}{\text{Time} \times \text{surface area}} \quad (3)$$

4.9 Quantification of evolved gases by GC

Gas evolution was measured in a gas-tight cell operated in a two-electrode configuration at the indicated bias (for unbiased operation, 0 V *vs.* the counter electrode, *e.g.*, Pt). The product compartment headspace was continuously purged with Ar carrier gas (10 sccm), and the outlet stream was fed to a gas chromatograph (DS Science) equipped with a thermal conductivity detector (TCD) and an MS-5A molecular-sieve column. The GC was calibrated using certified standards (H_2 3.9 vol% in Ar; O_2 21 vol% in air), and linear calibration curves were used to convert peak area to gas-phase mole fraction (y_i). The instantaneous molar production rate of species i was calculated as shown in eqn (4). Here, Q_{std} is the standard volumetric flow rate of the Ar carrier gas (in sccm, $cm^3\ min^{-1}$) referenced to the standard conditions defined by the mass-flow controller (STP). $V_{m,std}$ is the molar volume at those same standard conditions (*e.g.*, 22.414 $cm^3\ mol^{-1}$ at 0 °C, 1 atm; 24 465 $cm^3\ mol^{-1}$ at 25 °C, 1 atm).

$$n_i = y_i \times \left(\frac{Q_{\text{std}}}{V_{\text{m, std}}}\right) \quad (4)$$

The cumulative amount produced over a measurement window was obtained as in eqn (5).

$$N_i = \sum_k \left[y_{i(t_k)} \times \left(\frac{Q_{\text{std}}}{V_{\text{m, std}}}\right) \times \Delta t_k \right] \quad (5)$$

For comparison with electrochemical data, the total charge (C cm^{-2}) associated with the evolved gas was computed using eqn (6).

$$Q_i = \frac{(z \times F)}{(A \times N_i)} \quad (6)$$

4.10 Enzyme activity assay

We determined the activity of TsOYE spectrophotometrically by following the consumption of NADH at 340 nm.[37] We prepared TsOYE-containing KPi buffer (100 mM, pH 7.5) and irradiated it with simulated solar light (AM 1.5G, 100 mW cm^{-2}). After the irradiation, an aqueous solution containing 0.5 mM NADH and 10 mM 2-cyclohexen-1-one was mixed to estimate the OYE activity. The OYE-driven oxidation of NADH was monitored by

recording the time-dependent absorption spectrum at 340 nm using a V-650 spectrophotometer (JASCO). The enzymatic activity was calculated using eqn (4):

$$\text{Enzyme activity}\left(\text{mM s}^{-1}\right) = \frac{-\Delta A}{\Delta t} \times \frac{\text{dilution factor}}{\varepsilon \times l} \quad (7)$$

where $\Delta A/\Delta t$ is the initial slope of the time-dependent absorption spectrum at 0 s, ε is the extinction coefficient of NADH at 340 nm (6.22 mM^{-1} cm^{-1}), and l is the optical path length.

Author contributions

C. M. and B. S. conceived and designed the study. J. K., P. B., and G. K. A. prepared the halide perovskite cells, C. M. prepared the single-crystal TiO_2 protection layer, and C. M., C. H. K., and J. M. carried out the PEC and BPEC experiments. F. H. contributed samples for the BPEC experiments. C. M., H. H. P., C. B. P., and B. S. acquired funding for the research. B. S. and C. B. P, supervised the project. C. M. and C. H. K. drafted the manuscript, and all authors contributed to the revision and editing of the final version. All authors have read and approved the final manuscript.

Conflicts of interest

There are no conflicts to declare.

Data availability

The data supporting this article have been included as part of the supplementary information (SI). Supplementary information is available. See DOI: https://doi.org/10.1039/d5ta05513j.

Acknowledgements

This research was supported by the Basic Science Research Program through the National Research Foundation of Korea (NRF), funded by the Ministry of Education (No. 2022R1I1A1A01063534). This work was supported by the NRF grant funded by the Ministry of Strategy and Finance (No. 2021M3I3A1085009). This work was also supported by NRF grants funded by the Ministry of Science and ICT (No. RS-2023-00208832, RS-2023-00222078, RS-2024-00440681, RS-2024-00460425, NRF-2022K1A4A8A02079724).

References

1 M. R. Shaner, H. A. Atwater, N. S. Lewis and E. W. McFarland, *Energy Environ. Sci.*, 2016, **9**, 2354–2371.
2 B. A. Pinaud, J. D. Benck, L. C. Seitz, A. J. Forman, Z. Chen, T. G. Deutsch, B. D. James, K. N. Baum, G. N. Baum, S. Ardo, H. Wang, E. Miller and T. F. Jaramillo, *Energy Environ. Sci.*, 2013, **6**, 1983–2002.
3 D. Bae, B. Seger, P. C. K. Vesborg, O. Hansen and I. Chorkendorff, *Chem. Soc. Rev.*, 2017, **46**, 1933–1954.
4 S. Hu, N. S. Lewis, J. W. Ager, J. Yang, J. R. McKone and N. C. Strandwitz, *J. Phys. Chem. C*, 2015, **119**, 24201–24228.
5 D. Bae, T. Pedersen, B. Seger, B. Iandolo, O. Hansen, P. C. K. Vesborg and I. Chorkendorff, *Catal. Today*, 2017, **290**, 59–64.
6 H. J. Fu, I. A. Moreno-Hernandez, P. Buabthong, K. M. Papadantonakis, B. S. Brunschwig and N. S. Lewis, *Energy Environ. Sci.*, 2020, **13**, 4132–4141.
7 C. Moon, B. Seger, P. C. K. Vesborg, O. Hansen and I. Chorkendorff, *Cell Rep. Phys. Sci.*, 2020, **1**, 100261.
8 J. Choi, J. T. Song, H. S. Jang, M.-J. Choi, D. M. Sim, S. Yim, H. Lim, Y. S. Jung and J. Oh, *Electron. Mater. Lett.*, 2017, **13**, 57–65.
9 B. Koo, S.-W. Nam, R. Haight, S. Kim, S. Oh, M. Cho, J. Oh, J. Y. Lee, B. T. Ahn and B. Shin, *ACS Appl. Mater. Interfaces*, 2017, **9**, 5279–5287.
10 I. S. Kim, M. J. Pellin and A. B. F. Martinson, *ACS Energy Lett.*, 2019, **4**, 293–298.
11 M. Wang, B. Shi, Q. Zhang, X. Li, S. Pan, Y. Zhao and X. Zhang, *Sol. RRL*, 2022, **6**, 1–7.
12 V. Andrei, R. L. Z. Hoye, M. Crespo-Quesada, M. Bajada, S. Ahmad, M. De Volder, R. Friend and E. Reisner, *Adv. Energy Mater.*, 2018, **8**, 1–14.
13 J. Kim, S. Seo, J. Lee, H. Choi, S. Kim, G. Piao, Y. R. Kim, B. Park, J. Lee, Y. Jung, H. Park, S. Lee and K. Lee, *Adv. Funct. Mater.*, 2021, **31**, 2008277.
14 R. Tao, Z. Sun, F. Li, W. Fang and L. Xu, *ACS Appl. Energy Mater.*, 2019, **2**, 1969–1976.
15 H. Zhang, Z. Yang, W. Yu, H. Wang, W. Ma, X. Zong and C. Li, *Adv. Energy Mater.*, 2018, **8**, 1–7.
16 V. Andrei, G. M. Ucoski, C. Pornrungroj, C. Uswachoke, Q. Wang, D. S. Achilleos, H. Kasap, K. P. Sokol, R. A. Jagt, H. Lu, T. Lawson, A. Wagner, S. D. Pike, D. S. Wright, R. L. Z. Hoye, J. L. MacManus-Driscoll, H. J. Joyce, R. H. Friend and E. Reisner, *Nature*, 2022, **608**, 518–522.
17 V. Andrei, I. Roh, J. A. Lin, J. Lee, Y. Shan, C. K. Lin, S. Shelton, E. Reisner and P. Yang, *Nat. Catal.*, 2025, **8**, 137–146.
18 F. F. Abdi, R. R. Gutierrez Perez and S. Haussener, *Sustainable Energy Fuels*, 2020, **4**, 2734–2740.
19 J.-P. Becker, B. Turan, V. Smirnov, K. Welter, F. Urbain, J. Wolff, S. Haas and F. Finger, *J. Mater. Chem. A*, 2017, **5**, 4818–4826.
20 W. S. Knowles and R. Noyori, *Acc. Chem. Res.*, 2007, **40**, 1238–1239.
21 J. Kim and C. B. Park, *Curr. Opin. Chem. Biol.*, 2019, **49**, 122–129.
22 M. Mifsud, S. Gargiulo, S. Iborra, I. W. C. E. Arends, F. Hollmann and A. Corma, *Nat. Commun.*, 2014, **5**, 3145.
23 J. Kim, S. H. Lee, F. Tieves, C. E. Paul, F. Hollmann and C. B. Park, *Sci. Adv.*, 2019, **5**, eaax0501.
24 S. Takeuchi, T. Shimizu, T. Isaka, T. Tohei, N. Ikarashi and A. Sakai, *Sci. Rep.*, 2019, **9**, 2601.
25 I. Y. Choi, C. U. Kim, W. Park, H. Lee, M. H. Song, K. K. Hong, S. Il Seok and K. J. Choi, *Nano Energy*, 2019, **65**, 104044.
26 B. Koo, D. Kim, P. Boonmongkolras, S. R. Pae, S. Byun, J. Kim, J. H. Lee, D. H. Kim, S. Kim, B. T. Ahn, S.-W. Nam and B. Shin, *ACS Appl. Energy Mater.*, 2020, **3**, 2296–2303.

27 S. Geiger, O. Kasian, M. Ledendecker, E. Pizzutilo, A. M. Mingers, W. T. Fu, O. Diaz-Morales, Z. Li, T. Oellers, L. Fruchter, A. Ludwig, K. J. J. Mayrhofer, M. T. M. Koper and S. Cherevko, *Nat. Catal.*, 2018, **1**, 508–515.
28 C.-H. Yun, J. Kim, F. Hollmann and C. B. Park, *Chem. Sci.*, 2022, **13**, 12260–12279.
29 J. Yoon, H. Jang, M.-W. Oh, T. Hilberath, F. Hollmann, Y. S. Jung and C. B. Park, *Nat. Commun.*, 2022, **13**, 3741.
30 S. Bhattacharjee, M. Rahaman, V. Andrei, M. Miller, S. Rodríguez-Jiménez, E. Lam, C. Pornrungroj and E. Reisner, *Nat. Synth.*, 2023, **2**, 182–192.
31 S. Hao, H. Zhang, X. Sun, J. Chen, J. Zhai and S. Dong, *Appl. Catal. B Environ.*, 2024, **343**, 123481.
32 Y. Zhao, X. Zhao, K. Song, X. Sun, N. Xi, X. Zhang, Y. Sang, H. Liu and X. Yu, *Appl. Catal. B Environ. Energy*, 2024, **350**, 123901.
33 J. Kim and C. B. Park, *Chem Catal.*, 2022, **2**, 2425–2427.
34 D. H. Nam, G. M. Ryu, S. K. Kuk, D. S. Choi, E. J. Son and C. B. Park, *Appl. Catal. B Environ.*, 2016, **198**, 311–317.
35 E. J. Son, Y. W. Lee, J. W. Ko and C. B. Park, *ACS Sustain. Chem. Eng.*, 2019, **7**, 2545–2552.
36 S. Kara, D. Spickermann, J. H. Schrittwieser, C. Leggewie, W. J. H. van Berkel, I. W. C. E. Arends and F. Hollmann, *Green Chem.*, 2013, **15**, 330–335.
37 A. Riedel, M. Mehnert, C. E. Paul, A. H. Westphal, W. J. H. van Berkel and D. Tischler, *Front. Microbiol.*, 2015, **6**, 1073.

